Fish Physiol Biochem (2021) 47:1837–1849
https://doi.org/10.1007/s10695-021-01015-7

Zebrafish (*Danio rerio*) Oatp2b1 as a functional ortholog of the human OATP2B1 transporter

Jelena Dragojević · Nikola Marakovic · Marta Popović · Tvrtko Smital

Received: 26 March 2021 / Accepted: 3 September 2021 / Published online: 21 September 2021

Abstract OATP2B1 belongs to a highly conserved organic anion transporting polypeptide (OATP) family of transporters, involved in the cellular uptake of both endogenous and exogenous compounds. The reported substrates of human OATP2B1 include steroid conjugates, bile salts, and thyroid hormones, as well as pharmaceuticals. Human *OATP2B1* has orthologous genes in other vertebrate species, including zebrafish (*Danio rerio*), a widely used model organism in biomedical and environmental research. Our previous studies showed that zebrafish Oatp2b1 was phylogenetically closest to mammalian OATP2B1/Oatp2b1 and that it shares a similar tissue expression pattern. In this study, we aimed at discovering whether zebrafish Oatp2b1 could be a functional ortholog of human and rodent OATP2B1. To test this hypothesis, our primary goal was to obtain the first in vitro and in silico insights related to the structure and potential substrate preferences of zebrafish Oatp2b1. We generated cells transiently and stably transfected with zebrafish Oatp2b1 cloned from zebrafish liver, constructed an Oatp2b1 homology model, developed transport activity assays with model fluorescent substrate Lucifer yellow, and finally utilized this assay to analyze the interaction of zebrafish Oatp2b1 with both physiological and xenobiotic substances. Apart from structure similarities, our data revealed the strongest interaction of zebrafish Oatp2b1 with bile acids, steroid sulfates, thyroid hormones, and bilirubin, as well as xenobiotics bromosulfophthalein and sulfasalazine, which indicates its functional orthology with human OATP2B1.

Keywords OATP2b1/Oatp2b1 · Zebrafish · Transient and stable transfectants · Homology model · Substrate preferences · Functional orthology

Introduction

Members of the organic anion transporting polypeptide superfamily (OATP in humans and rodents/Oatp in other animals) are transmembrane proteins involved in the trafficking of large amphipathic molecules across the plasma membrane of eukaryotes. OATPs/Oatps mediate the transport of a wide range of endogenous (steroid hormones, bile salts, prostaglandins) and exogenous compounds (pharmaceuticals, natural toxins). Their role in ADME processes (absorption, distribution, metabolism, and

Supplementary Information The online version contains supplementary material available at https://doi.org/10.1007/s10695-021-01015-7.

J. Dragojević · M. Popović · T. Smital (✉)
Laboratory for Molecular Ecotoxicology, Division for Marine and Environmental Research, Ruđer Bošković Institute, Bijenička cesta 54, 10000 Zagreb, Croatia
e-mail: smital@irb.hr

N. Marakovic
Institute for Medical Research and Occupational Health, Ksaverska cesta 2, 10000 Zagreb, Croatia

elimination) has become increasingly recognized due to their involvement in the cellular uptake of drugs in tissues important for pharmacokinetics, such as the liver, kidney, and intestines (Kindla et al. 2009). Their high conservation across many species has been attributed to their central role in detoxification processes (Meier-Abt et al. 2006).

OATPs/Oatps have been classified into six subfamilies (OATP/Oatp1-6) with OATP1/Oatp1 members being the most extensively studied due to their link to human diseases and cancer treatment (Hagenbuch and Meier 2004; Hagenbuch and Stieger 2013). The OATP2/Oatp2 subfamily includes two transporters, OATP2A1 and OATP2B1, in humans, mice, and rats. OATP2B1, originally isolated from the human brain (Hagenbuch & Meier 2003; Kullak-Ublick et al. 2001; Tamai et al. 2000), is one of the most important members of the OATP/Oatp family, along with OATP1B1 and OATP1B3. It is a 709-amino acid glycoprotein containing 12 putative transmembrane-spanning domains (TMDs) (Hagenbuch and Meier 2004). Unlike other members of this sub-family, OATP2B1 is ubiquitously expressed across tissues in humans and rats. It is the third most expressed OATP in the basolateral hepatocyte membrane of the human liver (Kullak-Ublick et al. 2001; Tamai et al. 2000).

It has been shown that human OATP2B1 transports physiological substrates including steroid conjugates estrone 3-sulfate (E3S) and dehydroepiandrosterone sulfate (DHEAS), bile salt taurocholate, and thyroid hormone thyroxine (T4), as well as several pharmaceuticals like statins, fexofenadine, and glibenclamide (Hagenbuch and Gui 2008; Roth et al. 2012). A significant overlap in substrate specificities of OATP2B1 and the hepatic OATPs (OATP1B1 and OATP1B3) has been observed (McFeely et al. 2019). The transport mechanism has still not been resolved for OATP2B1. However, based on OATP1B1 and OATP2B1 homology models, it has been proposed that TMDs form a positively charged pore through which substrates are translocated. The mechanism of this translocation is termed the "rocker switch" — a conformational change from an outward- to an inward-facing topology elicited by the binding of a substrate molecule to specific residues within a substrate-binding pocket (Maier-Abt et al., 2005, Roth et al. 2012). OATP2B1 transport has been observed to be enhanced by acidic pH, and the possibilities of proton co-transport (alternatively, exchange with hydroxyl ions), the presence of a pH-sensitive active site on the transporters, and/or the increasing the turnover rate of the active sites across the membrane have been proposed (Nozawa et al. 2004; Sai et al. 2006).

In zebrafish, the Oatp superfamily consists of five families (Oatp1–5) that include 14 genes (Oatp1c1, Oatp1d1–2, Oatp1f1–4, Oatp2a1, Oatp2b1, Oatp3a1-2, Oatp4a1, and Oatp5a1–2), out of which six members are found only in the teleost fish lineage (Oatp1d1, Oatp1e1, and Oatp1f1–4) (Meier-Abt et al. 2005; Popovic et al. 2010). Tissue-specific gene expression, as determined by qPCR, revealed the highest expression of zebrafish Oatp2b1 in the gills of both sexes, followed by high expression in testes, and the brains, kidneys, and intestines of both sexes. Moderate expression of Oatp2b1 was observed in zebrafish ovaries and in the liver of males and females (Popovic 2014).

However, despite its expression in toxicologically relevant tissues most important for absorption, distribution, metabolism, and excretion (ADME) of xenobiotics (primarily liver, kidney, intestine, and gills) and its putative role in cellular detoxification, Oatp2b1 has been little studied in non-mammalian species. Given the high sequence and functional conservation of OATPs/Oatps across vertebrates and comparable expression patterns of fish and mammalian orthologs, we hypothesize that Oatp2b1 in zebrafish has a similar function to OATP2B1 in humans/mammals. Nevertheless, it is possible that functional orthology has been lost due to the whole genome duplication in teleost lineage or that function has been overtaken by other protein(s). Therefore, the primary goal of this study was to obtain initial in vitro and in silico insights into the structure, substrate preferences, and role of Oatp2b1 in zebrafish as a valuable model vertebrate species. To achieve this goal, we generated cells transiently and stably transfected with *oatp2b1* cloned from zebrafish liver, constructed a homology model of zebrafish Oatp2b1, developed transport activity assays using a model fluorescent substrate, and finally used this assay to analyze the interaction of Oatp2b1 with both physiological and xenobiotic substances.

Materials and methods

Chemicals

All of the tested compounds, model fluorescent substrates, and interactors alike were of the highest analytical grade and purchased from Sigma-Aldrich (Taufkirchen, Germany) or Alfa Aesar (Kandel, Germany).

Cloning and heterologous expression

A full-length zebrafish Oatp2b1 sequence was obtained from zebrafish cDNA by polymerase chain reaction using high fidelity Phusion DNA polymerase (Thermo Scientific, MA, USA) and specifically designed primers with NotI and HindIII restriction sites on the forward, and BgIII and XbaI restriction sites on the reverse primers. An amplified DNA fragment was cloned into a linearized pJET 2.0 vector (Invitrogen, Carlsbad, CA, USA). The sequence was verified by DNA sequencing using automated capillary electrophoresis (ABI PRISM® 3100-Avant Genetic Analyzer) at the Ruđer Bošković Institute DNA Service (Zagreb, Croatia). Sequenced genes of each clone were compared to the reported gene sequences from the NCBI and ENSEMBL databases. The verified sequence was subcloned into the pcDNA3.1(+) and pcDNA3.1/His vectors (Invitrogen). Transient transfection of human embryonic kidney cells (HEK293T) was based on a procedure previously described by Popovic et al. (2013) using polyethyleneimine (PEI) as the transfection reagent. To evaluate transfection efficiency, separate cells were transfected with pcDNA3.1/His/LacZ plasmid (Invitrogen) and transfection efficiency was evaluated 24 h after transfection with the LacZ staining protocol (Sambrook et al. 1989).

Stable expression of Oatp2b1 in genetically engineered HEK293Flp-In cells was achieved using targeted integration of Oatp2b1 sequence cloned into integration vector pcDNA5. pcDNA5/Oatp2b1 construct was specifically targeted into the genome of Flp-In-293 cell line following the manufacturer's instructions. In order to reach 90% confluence, Flp-In-cells were seeded in 6-well plates 48 h prior to transfection at a cell density of $3*10^5$ cells/cm^2, with a final volume of 2.5 mL per well. The transfection mixture consisted of 0.375 µg recombinant plasmid pcDNA5/FRT with inserted gene, 3.375 µg pOG44 plasmid, and 3.750 µg PEI reagent (1:1 ratio with pcDNA5/Frt + pOG44). pcDNA5-FRT/pOG44/PEI mixture (250 µL) was added to each well with 2.25 mL of DMEM medium without FBS and incubated for 4 h at 37 °C and 5% CO_2. After 4 h, the medium with transfection mixture was replaced with 2.5 mL DMEM-FBS per well. The transfected cells were left to grow in standard conditions for 48 h, scraped off, transferred to 25 cm^2 cell culture flask, and left to adhere overnight. The next morning, after the cells adhered to the flask bottom, 100 µg/mL of hygromycin B was added and the cells were kept in DMEM-FBS + hygromycin B for 20–25 days with DMEM-FBS change every 3–4 days. After that period, only transfected cells (i.e., hygromycin resistant) survived and started to grow. The cells were then tested for uptake of fluorescent substrates and later used for transport activity assays.

Western blotting and cell localization

Cells were collected from two wells of a 6-well microplate 24 h after transfection and lysed in NP-40 (Nonidet buffer) with a protease inhibitors cocktail AEBSF (Sigma-Aldrich, Taufkirchen, Germany) for 30 min on ice. After the lysis, cells were briefly sonicated (5 s at 5 µm) and centrifuged at 4000 × *g* for 20 min at 4 °C. Protein concentration in total cell lysate (TCL) was measured using Bradford assay (Bradford, 1976). Western blot analysis was performed using Mini-PROTEAN 3 Cell electrophoresis chamber for polyacrylamide gel electrophoresis, together with Mini Trans-Blot Cell transfer system (Bio-Rad Laboratories, CA, USA) for wet transfer. Proteins (20 µg per lane) were separated by electrophoresis in gradient (3–12%) polyacrylamide gel with 0.1% sodium dodecyl sulfate added and then transferred to the polyvinylidene difluoride membrane (Millipore, MA, US) via wet transfer (1 h at 80 V, with 0.025% SDS). Blocking was performed with low-fat milk 5% in TTBS for 1 h. Membranes were washed and incubated for 1 h with anti-Xpress antibody (Invitrogen, ThermoFisher Scientific, MA, USA) diluted 2500×. Goat anti-mouse IgG-HRP (diluted 5000×) was used as a secondary antibody with a 1-h incubation period (Santa Cruz Biotechnology, CA, USA). Histone H2B

antibody (Santa Cruz Biotechnology, INC) was used as the loading control. The proteins were visualized by chemiluminescence (Abcam, Cambridge, UK). Protein size was estimated by protein markers (ThermoFisher Scientific, MA, USA).

For immunofluorescence of Oatp2b1 protein expressed by transiently transfected plasmid, HEK293T cells were grown on glass coverslips in 24-well culture plates. Fixation of transiently transfected cells was performed with 3.7% formaldehyde in PBS during 25 min incubation. Cells were washed three times in 100 mM glycin/PBS, permeabilized with methanol for 15 min and washed 3 times in PBS. Antigen retrieval was done in 1% SDS/PBS for 5 min. Cells were then blocked in 5% low-fat milk for 30 min with gentle agitation at room temperature. Subsequently, coverslips were transferred on microscope slides and incubated with Anti-Xpress antibody (1:100) (Invitrogen, ThermoFisher Scientific, MA, USA) in blocking solution for 1 h at 37 °C in humidity chamber, washed, and incubated with secondary FITC antibody (Santa Cruz Biotechnology, CA, USA) (1:100) in blocking solution for 1 h at 37 °C. When double staining was performed after incubation with FITC, blocking was done in 5% low-fat milk for 30 min with gentle agitation, followed by incubation with Na, K-ATPase anti-mouse primary antibody for 2 h (1:150), washing, and 1 h incubation with Cy3-conjugated anti-mouse IgG-HRP (Santa Cruz Biotechnology, CA, USA) as a secondary antibody (1:200). Nuclei were stained with 300 nM DAPI/PBS for 45 min at 37 °C. After mounting the samples in Fluoromount medium, immunofluorescence was detected using confocal microscope Leica TCS SP2 AOBS (Leica Microsystems, Wetzlar, Germany).

Homology modeling — human vs. zebrafish OATP2b1/Oatp2b1

Build Homology Models protocol as implemented in Biovia Discovery Studio Client v18.1. (Dassault Systèmes, Vélizy-Villacoublay, France) was used to construct both human and *Danio rerio* OATP2b1/Oatp2b1 homology models based on the alignment of the model sequence and the template structure — crystal structure of the glycerol-3-phosphate transporter from *Escherichia coli* (PDB ID: 1pw4) (F. Meier-Abt et al., 2006, Huang et al., 2003). To generate homology models, the Build Homology Models protocol uses the MODELER (Sali and Blundell, 1993) automodel. The input sequence alignment between the model sequence of the corresponding Oatp2b1 and the sequence of glycerol-3-phosphate transporter, necessary for building the homology model, was obtained using Align Sequences protocol (for hsOATP2b1, Sequence Identity: 10.3%, Sequence Similarity: 30,8%; for drOatp2b1, Sequence Identity: 9.6%, Sequence Similarity: 28,4%). After alignment analysis, long insertions that could not be modeled correctly were excised in order to obtain a reliable model. All insertions (the N-terminal variable region, the large extracellular and intracellular loops/regions) that were deemed to be unreliable were excised/removed. A structure-based sequence alignment of corresponding Oatp2b1 and glycerol-3-phosphate transporter template with the unmodeled extracellular and intracellular portions illustrated (underlined) are shown in Figures S5 and S6 in the Supplementary Material.

The remaining parameters in the Parameters Explorer of the Build Homology Models protocol were set as follows. Cut Overhangs was set to True to cut the terminal residues of the input model sequence that were not aligned with the templates. Number of Models was set to 10 to specify the number of models created from an initial structure. Optimization Level was set to High to define the proportion of performed molecular dynamics with simulated annealing. As to building refinement models on detected loop regions, i.e., the model sequence regions of at least five residues length which are not aligned with the template, Refine Loops was set to True. Build Homology Models protocol uses the DOPE (Discrete Optimized Protein Energy) (Shen and Sali, 2006) method to refine loops. Refine Loops Number of Models was set to 5 to define the number of models to be created by loop optimization, and Refine Loops Optimization Level was set to Low to define the number of models to be created by loop optimization. Refine Loops with Use Discrete Optimized Protein Energy (DOPE) Method was set to High Resolution.

After running Build Homology Models protocol, the Best Model Structure Superimposed to Templates was selected from the generated output models for the final three-dimensional model structure of Oatp1d1. Finally, the selected model was manually adjusted and minimized using Smart Minimizer algorithm. The dielectric constant to be used to minimize the

OATP2b1/Oatp2b1 models was set to 2 corresponding to the dielectric properties of saturated hydrocarbons as instructed when modeling a membrane system. Dock Ligands (CDOCKER) protocol using full potential CHARMm force field for atom typing for docking Lucifer yellow inside a binding site defined as a sphere large enough to surround a central pore of corresponding Oatp2b1 homology model. The final pose representing predicted binding conformation of Lucifer yellow inside corresponding Oatp2b1 structure was selected based on the highest frequency among all generated poses (Fig. 7).

Transport activity assays

FlpIn/Oatp2b1 cells were grown in 96-well plates (density $8*10^5$ cells/mL) for 24 h until they reached confluency. DMEM/FBS was removed and cells were preincubated in 100 µL of the transport medium (145 mM NaCl, 3 mM KCl, 1 mM $CaCl_2$, 5 mM glucose, 5 mM HEPES, and 0.5 mM $MgCl_2$) for 10 min at 37 °C. To assess the transport and dose response rates of fluorescent substrate LY, 25 µL of five times concentrated fluorescent substrate was added to the preincubation medium and incubated for 2.5 min at 37 °C. The concentration range applied was 1–500 µM. Incubation time was determined based on the initial time response experiments (Fig. S1 in Supplementary Material). After the incubation, the cells were washed two times with 125 µL of cold transport medium and lysed with 0.1% of sodium dodecyl sulfate (SDS) for 30 min. Lysed cells were transferred to the 96-well black plates and the fluorescence was measured with a microplate reader (Infinite M200, Tecan, Salzburg, Austria). The transport rates were determined by subtracting the measured fluorescence of transfected cells with the fluorescence of non-transfected control cells. Normalization of the obtained fluorescence response was done using calibration curves obtained for each substrate, taking into account protein content. Calibration curves for fluorescent dyes were generated in 0.1% SDS and in the cell matrix dissolved in 0.1% SDS. Total protein concentration was measured using the Bradford assay (Bradford, 1976). Using the calibration curves and total protein content, the uptake of the fluorescent substrates was expressed as nM of substrates per mg of protein per minute. After determination of transport kinetics for fluorescent dye, LY was used in subsequent inhibition assays. Inhibition measurements were based on the co-exposure of transfected cells and mock control with the determined model substrate and potential interactor. After 10 min of incubation, cells were incubated for 40 s with the test compounds, followed by 2.5 min incubation with LY. The concentration of model substrate used was in the linear part of the previously determined concentration–response curve. The interaction screens were initially performed with one concentration of tested compounds (100 µM), and for the most potent interactors, detailed dose response experiments were performed and the respective IC_{50} values determined.

Type of interaction for the strongest interactors identified in the initial interaction screening was determined by comparing the kinetic parameters of LY uptake in the presence and absence of interacting compounds, where their concentrations corresponded to their previously calculated IC_{50} values. A competitive inhibitor (i.e., substrate) will cause an increase in K_m, but leave V_{max} unaffected. The presence of a non-competitive inhibitor will decrease V_{max} and will not affect K_m. A third type of interaction is uncompetitive inhibition, where both V_{max} and K_m are decreased.

Results

Protein identification and cell localization

Western blot analysis of total cell lysate from HEK293/Oatp2b1 overexpressing cells revealed two distinct signals, a monomeric form of approximately 80 kDa and an oligomeric band at > 200 kDa, with possible post-translational modifications seen as smears above the monomeric and oligomeric bands. Histone H2B (18 kDa) served as a loading control (Fig. 1).

Immunofluorescence showed localization of zebrafish Oatp2b1 within the cell membrane of transiently transfected HEK293T cells. This was visualized by co-localization of green-stained Oatp2b1 (FITC) and red-stained Na/K ATPase (CY3), which is normally localized in the cell membrane. As a result of co-localization, the signals from the two dyes were combined and subsequently produced an orange signal that confirmed the localization of zebrafish Oatp2b1 within the cell membrane (Fig. 2). This result indicates that the zebrafish Oatp2b1 protein

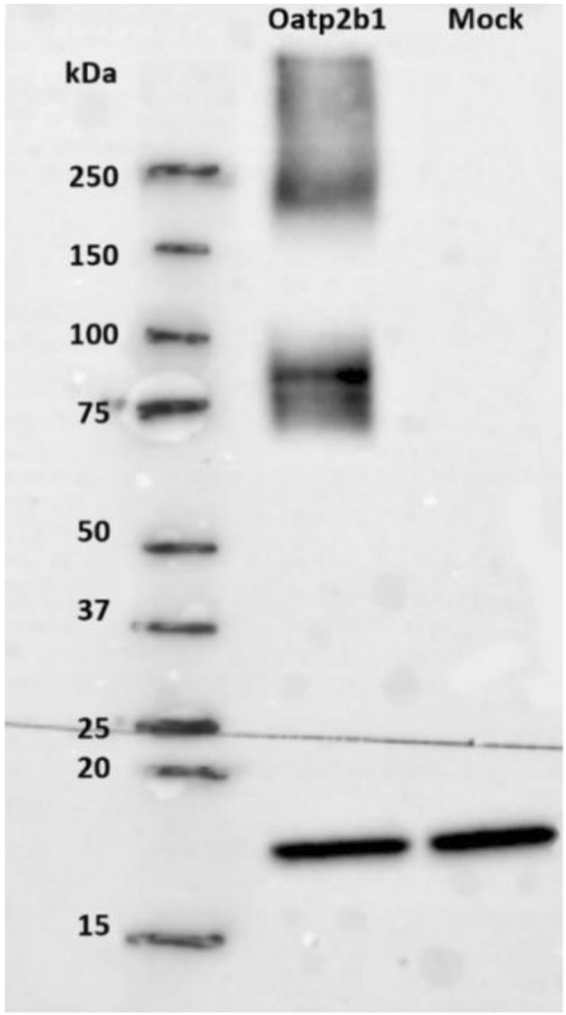

Fig. 1 Western blot analysis of zebrafish Oatp2b1 transporter expressed in transfected versus mock transfected cells. Total cell lysate revealed Oatp2b1 protein bands that corresponds to the size of glycosylated monomeric protein and possible homo- or heterodimeric forms and post-translational modifications, respectively

is correctly localized and can be functional in the expression system used.

Homology modeling — human vs. zebrafish Oatp2b1

The generated models of human OATP2b1 and zebrafish Oatp2b1 are shown in Figs. 3 and 4, respectively. Since they start from the same template structure (glycerol-3-phosphate transporter from *E. coli*), a high similarity between the global structure of the two models is expected. Indeed, the molecular overlay revealed a high degree of similarity with an overlay similarity ratio of 0.629017. Closer inspection revealed that the shortest distance between the residues defining the diameter of the active site at the closed end of the substrate-translocation pathway in the middle of the membrane is predicted to be shorter in the case of zebrafish Oatp2b1 (12.6 Å vs. 13.6 Å in the case of human OATP2B1). This is in consistent with the negligibly larger solvent-accessible surface within the active site in the case of human OATP2B1.

Furthermore, using molecular docking, we generated model complexes of the structural model of human or *Danio rerio* OATP2b1/Oatp2b1 and known model substrate LY (Fig. 5) with a binding sphere ($r = 24.1$ and 24.7 Å, respectively) defined large enough to encompass most of the central pore. For both models, LY is predicted to be positioned in the center of the transmembrane channel, confirming the quality of the generated models.

Functional characterization of zebrafish Oatp2b1

Model substrate

Initial testing of anionic fluorescent dyes that could be used as substrates for functional characterization of zebrafish Oatp2b1 revealed Lucifer yellow (LY) as a potential fluorescent substrate under physiological conditions (pH 7.4). Time- and dose–response assays confirmed that LY is indeed an Oatp2b1 substrate and its transport followed classical Michaelis–Menten kinetics (Fig. 6). The determined kinetic parameters of the LY transport in transfected cells at pH 7.4 resulted in a V_{max} value of 21.4 nmol/mg protein/min and K_m of 620.3 µM (Fig. 6).

However, because human/mammalian OATP2B1/Oatp2b1 shows increased transport activity at acidic pH, we performed an uptake transport assay with LY also in acidic conditions (pH 5), which indeed resulted in an increased transport rate of LY ($V_{max} = 51.5$ nmol/mg protein/min, $K_m = 175.8$ µM; Fig. 7).

Interaction screening

Due to the fact that mammalian OATP2B1 exhibits increased transport activity and increased substrate recognition at acidic pH, we decided to perform interaction experiments under acidic conditions (pH 5).

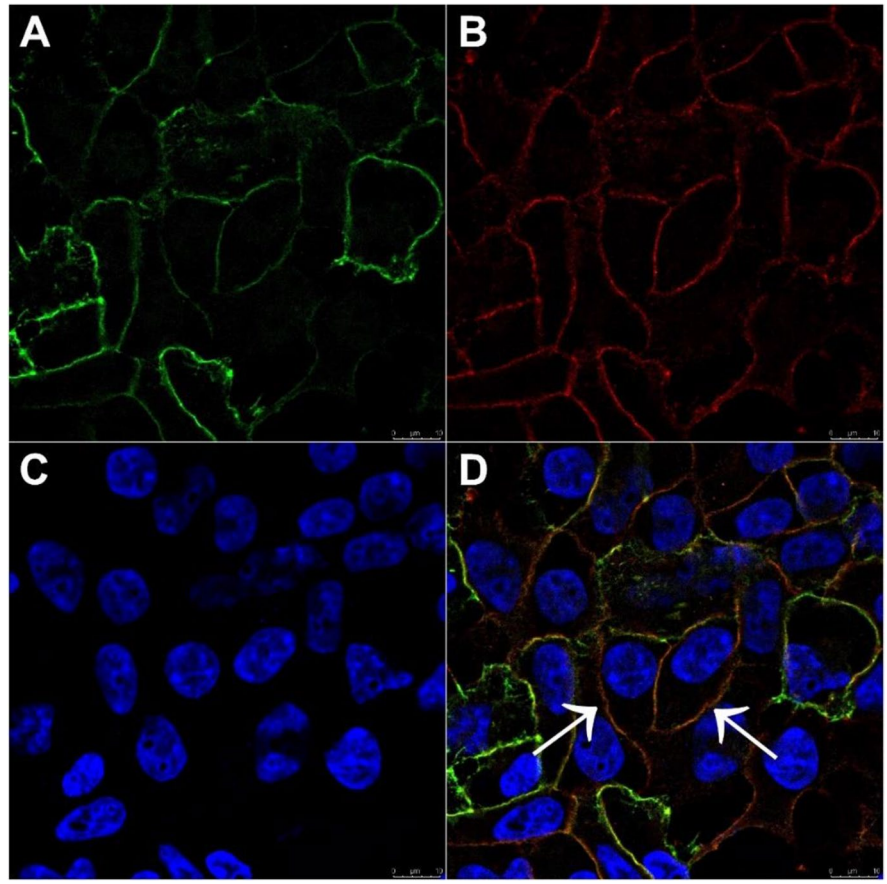

Fig. 2 Immunolocalization of zebrafish Oatp2b1 by co-localization of the green-colored Oatp2b1 and the red-colored Na/K ATPase. The signals of the two dyes were combined, resulting in an orange signal which confirmed the localization within the cell membrane. Nuclei are stained with DAPI (blue)

The initial screening revealed interactions with a wide range of physiological compounds as well as xenobiotics, confirming the polyspecific substrate specificity of zebrafish Oatp2b1 (Fig. 8). It showed major interactions with steroid and thyroid hormones and bilirubin. The strongest interaction was observed with bilirubin, resulting in complete inhibition of LY uptake upon co-exposure of Oatp2b1 transfected cells to 100 µM bilirubin. Triiodothyronine (T3), pregnenolone sulfate, T4, ethynyltestosterone, progesterone, and 17α-ethynylestradiol also strongly inhibited Oatp2b1 transport, resulting in only 1.8%, 4.6%, 7.2%, 11.7%, 12.6%, and 17% LY uptake remaining in comparison to the control (100%), respectively. From the group of xenobiotics, the strongest interaction was seen with bromosulfophthalein (BSP), perfluorooctanesulfonic acid (PFOS), diclofenac, perfluorooctanoic acid (PFOA), atorvastatin, and tetracycline (0%, 1.8%, 2.5%, 7%, 14.5%, and 15.1%, respectively).

Dose–response assays

After the initial screening of the described series of compounds, the most potent interactors were selected for detailed dose–response analyses and determination of their IC_{50} values. Oatp2b1 showed the strongest interaction with cholic acid (IC_{50} = 0.7 µM), BSP (IC_{50} = 0.83 µM), and pregnenolone sulfate (IC_{50} = 4.99 µM). Other compounds that inhibited the uptake of LY by more than 80% were PFOS, diclofenac, and sulfasalazine with IC_{50} values of 11.93, 13.16, and 15.75, respectively (Table 1; Fig. S2 and Fig. S3 in Supplementary Material).

Determining the type of interaction

Following determination of IC_{50} values, the type of interaction for the strongest Oatp2b1 interactors was determined using Michaelis–Menten kinetics determinations (Table 1, Fig. S4 in Supplementary

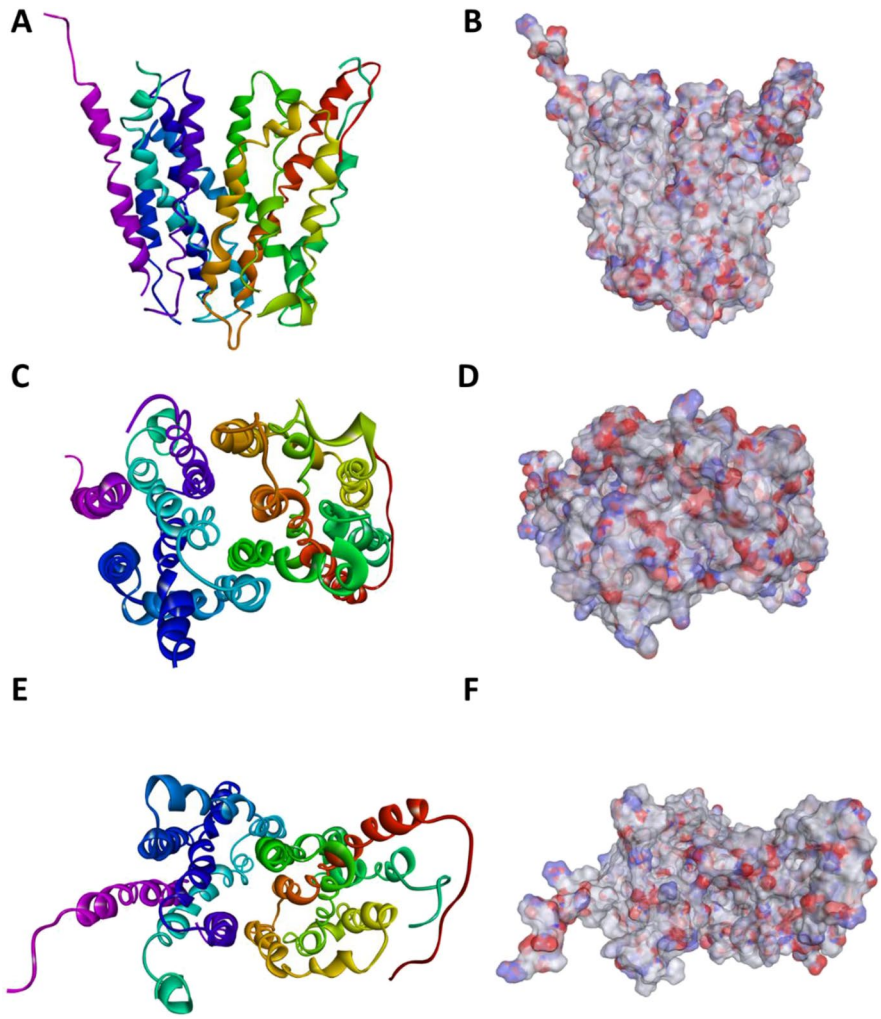

Fig. 3 Solid ribbon and rainbow-colored representation of the homology model of human OATP2b1 as viewed from the lateral side (**A**), the extracellular side (**C**), and the intracellular side (**E**) with electrostatic potential mapped onto its molecular surface, respectively (**B**, **D**, **F**). Regions of negative, positive, and neutral potential are shown in red, blue, and white/gray, respectively

Material). BSP and pregnonolone sulfate were identified as substrates, whereas diclofenac and PFOS were found to be inhibitors of Oatp2b1.

Discussion

The data shown in this study represent the first insights into the structure, substrate preferences, and possible function of zebrafish Oatp2b1. The transporter was first identified and classified in 2010 by Popovic et al. It showed ubiquitously high expression with a tissue expression pattern similar to that of OATP2B1 in mice. Analysis of membrane topology revealed a high probability that zebrafish Oatps have 12 TMDs and that the organization of TMDs and LPs is highly conserved. Conserved motifs specific for the OATP superfamily were also identified in zebrafish Oatps: the superfamily signature, a large extracellular loop 5 with ten conserved cysteines, and the Kazal SLC21 domain. Human OATP2B1 is a 709 amino acid and 85 kDa large glycoprotein containing 12 putative transmembrane spanning domains (Hagenbuch, 2004; Grube et al. 2006). As indicated by western blot analysis, the zebrafish Oatp2b1 protein obtained in this study was approximately 85 kDa in size, which corresponds to the size of human OATP2B1. However, because the predicted protein size is 75 kDa, based on the nucleotide sequence, we suggest that zebrafish Oatp2b1 is most likely glycosylated. Based on the amino acid structure of zebrafish Oatp2b1 (NetNGlyc 1.0 server), there are four predicted N-glycosylation sites: N131, N149, N474, and N673. N-glycosylation may be important

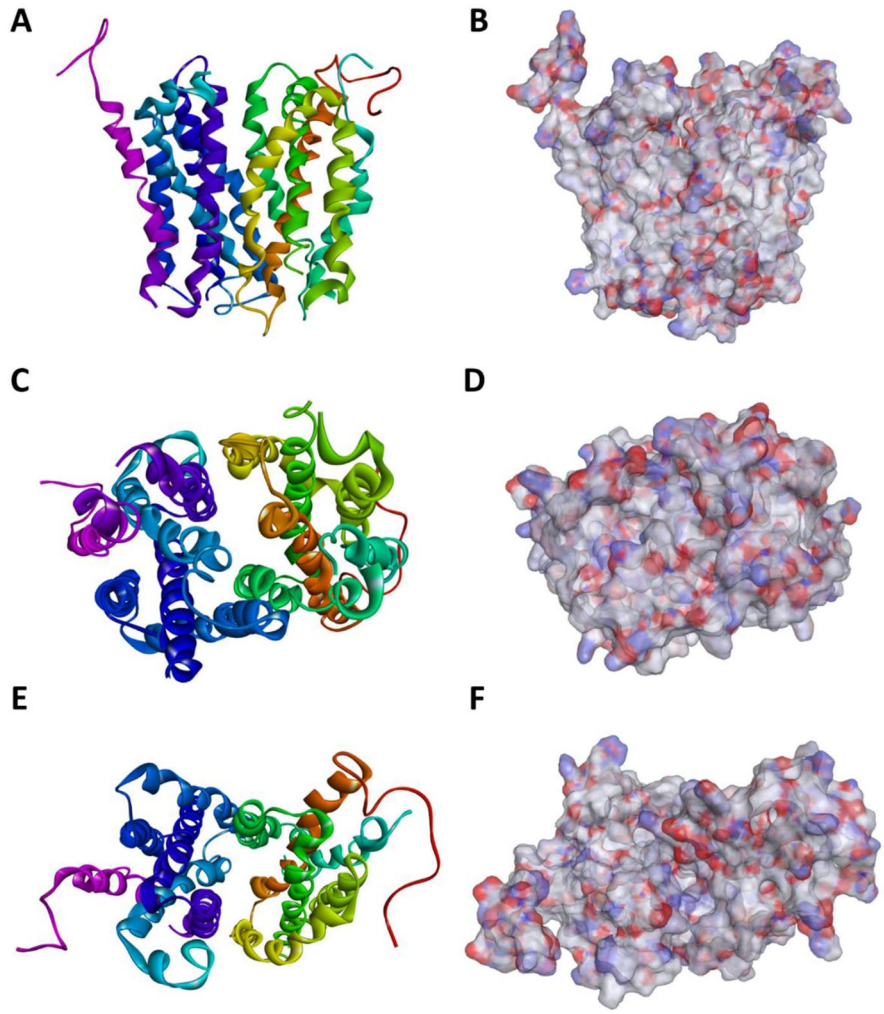

Fig. 4 Solid ribbon and rainbow-colored representation of the homology model of zebrafish Oatp2b1 as viewed from the lateral side (**A**), the extracellular side (**C**), and the intracellular side (**E**) with electrostatic potential mapped onto its molecular surface, respectively (**B**, **D**, **F**). Regions of negative, positive, and neutral potential are shown in red, blue, and white/gray, respectively

for membrane localization, similarly to what has been shown for another zebrafish Oatp, the teleost-specific Oatp1d1 (Popovic et al. 2013). Our immunofluorescence analysis clearly showed localization of Oatp2b1 inside the membrane of transiently transfected HEK293T cells, indicating that it is correctly localized and likely functionally active in the expression system used. Several other immunolocalization studies have also shown that OATP2B1 is mainly expressed in the plasma membrane (Kindla et al. 2011; Kleberg et al. 2012; Knauer et al., 2010; Le Vee et al. 2013).

Crystal structures are not yet available for any OATP/Oatp transporter. However, comparison of the in silico predicted protein structures a human OATP2b1 and zebrafish Oatp2b1 performed in this study (Figs. 3 and 4) clearly shows significant similarities between the two transporters, which is further supported by successful molecular docking of the model substrate LY (Fig. 5). However, closer inspection reveals that LY is predicted to be placed slightly lower in the central pore in the case of zebrafish. A possible explanation could be inferred from the aforementioned slightly narrower central pore in the case of zebrafish Oat2b1, where a more constricted channel providing a more secure fit around the substrate molecule could more easily guide LY through the channel in a directional manner, providing less space available for substrate rotation to cause its retention. Taken together, while constructed homology models cannot provide the same level of confidence and insight that can be

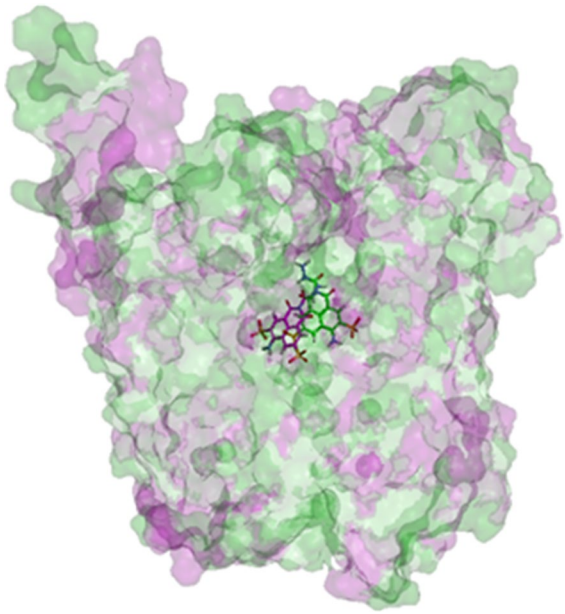

Fig. 5 Superposition of model complexes between human OATP2b1 (carbon atoms in green) or zebrafish Oatp2b1 (carbon atoms in magenta) and LY, respectively

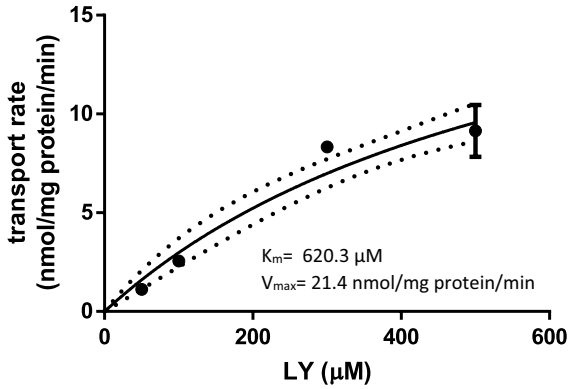

Fig. 6 Dose–response of zebrafish Oatp2b1 transport of the fluorescent model substrate LY (K_m = 620.3 μM) expressed as transport rate (nmol/mg protein/min) over LY concentration (μM) after 2.5 min incubation with LY at pH 7.4. Each data point represents the mean ± SE from triplicate determinations. Dotted lines represent confidence intervals

obtained by protein crystallography, we believe that the models obtained in this study can be used for further molecular docking studies aimed at determining interactions of OATP2b1/Oatp2b1 with various physiological and xenobiotic substances.

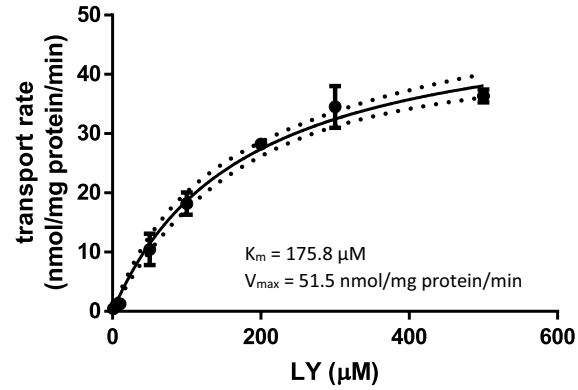

Fig. 7 Dose–response of zebrafish Oatp2b1 transport of the fluorescent model substrate LY (K_m = 175.8 μM) expressed as transport rate (nmol/mg protein/min) over LY concentration (μM) after 2.5 min incubation with LY at pH 5. Each data point represents the mean ± SE from triplicate determinations. Dotted lines represent confidence intervals

After identifying the zebrafish Oatp2b1 protein and confirming its correct localization in HEK293T cell membranes, we verified LY as a model fluorescent substrate that can be used in transport activity assays and subsequent high-throughput screening protocols to gain better insights into zebrafish Oatp2b1 interaction preferences. LY showed high accumulation in transfected cells and followed classical Michaelis–Menten kinetics. Considering that human OATP2B1 shows pH-dependent transport activity, with increased transport activity observed at acidic pH, we tested transport of the model substrate in both physiological (pH 7.4) and acidic conditions (pH 5). Similar to what has been reported for human OATP2B1, we observed an increase in LY transport under acidic conditions (Fig. 7). The pH dependence of OATP2B1 is considered to be driven by the proton gradient, which likely plays a physiological role in the uptake of compounds from the intestinal lumen where pH is weakly acidic (Tamai 2012). Furthermore, several mutagenesis studies have shown that pH dependence is likely associated with a highly conserved histidine in the third transmembrane domain (Leuthold et al. 2009; Hagenbuch and Stieger 2013).

Based on the expression profile and phylogenetic analysis which showed that zebrafish Oatp2b1 is phylogenetically closest to mammalian OATP2B1/Oatp2b1, Popovic et al. (2010) suggested that it may be a functional ortholog of OATP2B1. Based on this presumption, we tested some of the OATP2B1

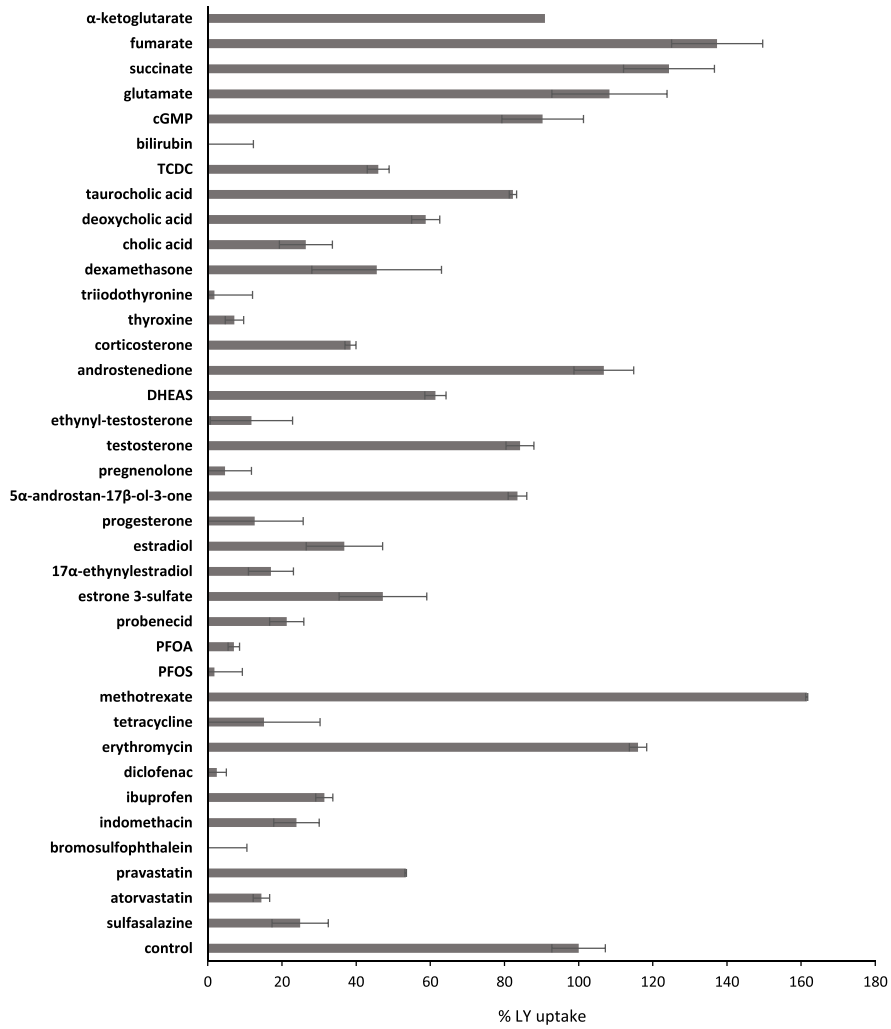

Fig. 8 Interaction of zebrafish Oatp2b1 with known interactors of mammalian Oatp subfamily members and similar anionic compounds. Data are expressed as mean percentage (%) ± SD from triplicate determinations of LY uptake after co-incubation with each interactor (100 µM) relative to LY uptake in the absence of an interactor which is set to 100% (control)

Table 1 Overview of kinetic parameters and types of interaction determined for the strongest interactors of zebrafish Oatp2b1

	IC_{50} (µM)	V_{max}	c.i	K_m	c.i	toi*
Control (LY)		51.45	45.69–57.2	175,8	128 – 223.5	
Bilirubin	34.26	-	-	-	-	-
Sulfasalazine	15.75	-	-	-	-	-
17α-Ethynylestradiol	34.46	-	-	-	-	-
Diclofenac	13.16	23.8	10.97–36.62	342.7	0.0–690.6	I
Ibuprofen	49.45	-	-	-	-	-
PFOA	24.75	-	-	-	-	-
PFOS	11.93	32.14	20.47–43.8	297.7	89.95–505.3	I
BSP	0.83	45.09	27.65–62.54	594.2	233.6–954.8	S
Pregnenolone sulfate	4.99	71.51	42.07–101.0	877.7	369.3–1386	S
Cholic acid	0.7	-	-	-	-	-

*toi, type of interaction.

interactors and similar anionic compounds for interaction with zebrafish Oatp2b1. Because human OATP2B1 showed an increase in transport activity and number of substrates recognized at acidic pH, we performed the initial interaction screening at pH 5. Within the potential physiological substrates, we observed the highest interaction with cholic acid, pregnenolone sulfate, and bilirubin. The interaction with bile acids, steroid sulfates, and thyroid hormones as well as bilirubin indicates a functional similarity with OATP2B1 (Al Sarakbi et al. 2006; Bronger et al. 2005; Köck et al. 2010). Since the majority of endogenous substrates of human OATP2B1 are steroid hormones and bile acids, its presumed physiological role is to help in the distribution and elimination of regulatory compounds. Based on our results, this may also be the case for zebrafish Oatp2b1, although further studies and testing with a higher number of substances should be performed to confirm this hypothesis.

On the other hand, the xenobiotics that showed the strongest interaction with zebrafish Oatp2b1 were BSP, PFOS, diclofenac, and sulfasalazine, and BSP was identified as a substrate. BSP and sulfasalazine are also high-affinity substrates of human OATP2B1 with a determined K_m value of 0.7 µM (Kullak-Ublick et al. 2001) and 1.7 µM (Kusuhara et al. 2012), respectively. In addition, we identified ibuprofen and PFOS as inhibitors of Oatp2b1. No specific inhibitors have yet been identified for human OATP2B1, although aliskiren, celiprolol, and pemetrexed may be candidates as they are selective substrates (McFeely et al. 2019).

In summary, based on the interaction data observed in this study, we suggest that zebrafish Oatp2b1 may indeed be a functional ortholog of human OATP2B1. Nevertheless, there are still many gaps in our knowledge regarding data on the expression, localization, regulation, and function of Oatp2b1, particularly in non-mammalian species, including fish. Moreover, it is important to note that the focus of regulatory agencies worldwide has been primarily on hepatic OATPs, particularly 1B1 and 1B3 (Mcfeely et al. 2019). As more and more studies emerge, highlighting the importance of OATP transporters in the uptake and disposition of many endobiotics and xenobiotics, including drugs, it has become obvious that more research should be directed towards these types of transporters. The same is true for Oatp2b1 in zebrafish, as it is the second most abundantly expressed Oatp in zebrafish liver. In addition to its highly probable physiological role, Oatp2b1 could be an integral component of cellular defense and its inhibition by environmental pollutants could be of considerable ecotoxicological relevance. Therefore, this study could serve as a basis for further toxicological and environmental research on the importance of Oatp2b1-mediated uptake of drugs, endo- and xenobiotics in zebrafish as an important vertebrate model species.

Author contribution JD designed and performed majority of cloning, transfection, and interaction experiments and wrote the manuscript; NM performed homology modeling and molecular docking studies; MP did initial cloning of zebrafish Oatp2b1; TS supervised the project, study conception, and design and wrote the manuscript with input from all authors. All of the authors reviewed the results and approved the final version of the manuscript.

Funding This study was financed by the Croatian Science Foundation (Project No. IP-2019–04-1147) and partially supported under the STIM-REI project, Contract Number: KK.01.1.1.01.0003, a project funded by the European Union through the European Regional Development Fund – Operational Programme Competitiveness and Cohesion 2014–2020 (KK.01.1.1.01). The computational resources and Biovia Discovery Studio Client v18.1 software (Dassault Systèmes, Vélizy-Villacoublay, France), used for homology modeling and molecular docking studies, were provided through Croatian Science Foundation projects (grant numbers HrZZ-IP-2013–11-4307 and HrZZ-IP-2018–01-7683).

Data availability The datasets generated during and/or analyzed during the current study are available from the corresponding author on reasonable request.

Code availability Not applicable.

Declarations

Ethics approval Not applicable.

Consent to participate Not applicable.

Consent for publication Not applicable.

Conflict of interest The authors declare no competing interests.

References

Al Sarakbi W, Mokbel R, Salhab M, Jiang WG, Reed MJ, Mokbel K (2006) The role of STS and OATP-B mRNA expression in predicting the clinical outcome in human breast cancer. Anticancer Res 26:4985–4990

Bronger H, König J, Kopplow K, Steiner HH, Ahmadi R, Herold-Mende C (2005) ABCC drug efflux pumps and organic anion uptake transporters in human gliomas and the blood-tumor barrier. Cancer Res 65:11419–11428

Grube M, Köck K, Oswald S, Draber K, Meissner K, Eckel L, Böhm M, Felix SB, Vogelgesang S, Jedlitschky G, Siegmund W, Warzok R, Kroemer HK (2006) Organic anion transporting polypeptide 2B1 is a high-affinity transporter for atorvastatin and is expressed in the human heart. Clin Pharmacol Ther 80:607–620

Hagenbuch B, Gui C (2008) Xenobiotic transporters of the human organic anion transporting polypeptides (OATP) family. Xenobiotica 38:778–801

Hagenbuch B, Meier PJ (2003) The superfamily of organic anion transporting polypeptides. BBA Biomem 1609:1–18

Hagenbuch B, Meier PJ (2004) Organic anion transporting polypeptides of the OATP/SLC21 family: phylogenetic classification as OATP/SLCO superfamily, new nomenclature and molecular/functional properties. Pflugers Arch 447:653–665

Hagenbuch B, Stieger B (2013) Molecular Aspects of Medicine The SLCO (former SLC21) superfamily of transporters. Mol Aspects Med 34:396–412

Kindla J, Fromm MF, König J (2009) *In vitro* evidence for the role of OATP and OCT uptake transporters in drug–drug interactions. Exp Opin Drug Metab Toxicol 5:489–500

Kindla J, Rau TT, Jung R, Fasching PA, Strick R, Stoehr R (2011) Expression and localization of the uptake transporters OATP2B1, OATP3A1 and OATP5A1 in non-malignant and malignant breast tissue. Cancer Biol Ther 11:584–591

Kleberg K, Jensen GM, Christensen DP, Lundh M, Grunnet LG, Knuhtsen S, Poulsen SS, Berner Hansen M, Bindslev N (2012) Transporter function and AMP turnover in normal colonic mucosa from patients with and without colorectal neoplasia. BMC Gastroenter 12:78

Köck K, Koenen A, Giese B, Fraunholz M, May K, Siegmund W, Hammer E, Völker U, Jedlitschky G, Kroemer HK, Grube M (2010) Rapid modulation of the organic anion transporting polypeptide 2B1 (OATP2B1, SLCO2B1) function by protein kinase C-mediated internalization. J Biol Chem 285:11336–11347

Kullak-Ublick GA, Ismair MG, Stieger B, Landmann L, Huber R, Pizzagalli F, Fattinger K, Meier PJ, Hagenbuch B (2001) Organic anion-transporting polypeptide B (OATP-B) and its functional comparison with three other OATPs of human liver. Gastroenter 120:525–533

Kusuhara H, Furuie H, Inano A, Sunagawa A, Yamada S, Wu C, Fukizawa S, Morimoto N, Ieiri I, Morishita M, Sumita K, Mayahara H, Fujita T, Maeda K, Sugiyama Y (2012) Pharmacokinetic interaction study of sulphasalazine in healthy subjects and the impact of curcumin as an in vivo inhibitor of BCRP. Br J Pharmacol 166:1793–1803

Le Vee M, Noel G, Jouan E, Stieger B, Fardel O (2013) Polarized expression of drug transporters in differentiated human hepatoma HepaRG cells. Toxicol in Vitro 27:1979–1986

Leuthold S, Hagenbuch B, Mohebbi N, Wagner CA, Meier PJ, Stieger B (2009) Mechanisms of pH-gradient driven transport mediated by organic anion polypeptide transporters. Am J Physiol Cell Physiol 296:C570-582

McFeely SJ, Wu L, Ritchie TK, Unadkat J (2019) Organic anion transporting polypeptide 2B1 – more than a glass-full of drug interactions. Pharmacol Ther 196:204–215

Meier-Abt F, Mokrab Y, Mizuguchi K (2005) Organic anion transporting polypeptides of the OATP/SLCO superfamily: identification of new members in nonmammalian species, comparative modeling and a potential transport mode. J Membr Biol 208:213–227

Nozawa T, Imai K, Nezu JI, Tsuji A, Tamai I (2004) Functional characterization of pH sensitive organic anion transporting polypeptide OATP-B in human. J Pharmacol Exp Ther 308:438–445

Popovic M (2014) Identification, characterization and ecotoxicological relevance of membrane transport protein families Slc21 and Slc22 in zebrafish (*Danio rerio* Hamilton, 1822). PhD thesis. Josip Juraj Strossmayer University of Osijek.

Popovic M, Zaja R, Fent K, Smital T (2013) Molecular characterization of zebrafish Oatp1d1 (Slco1d1), a novel Organic anion transporting polypeptide. J Biol Chem 288:33894–33911

Popovic M, Zaja R, Smital T (2010) Organic anion transporting polypeptides (OATP) in zebrafish (*Danio rerio*): phylogenetic analysis and tissue distribution. Comp Biochem Physiol A 155:327–335

Roth M, Obaidat A, Hagenbuch B (2012) OATPs, OATs and OCTs: the organic anion and cation transporters of the SLCO and SLC22A gene superfamilies. Br J Pharmacol 165:1260–1287

Sai Y, Kaneko Y, Ito S, Mitsuoka K, Kato Y, Tamai I, Artursson P, Tsuji A (2006) Predominant contribution of organic anion transporting polypeptide OATP-B (OATP2B1) to apical uptake of estrone-3-sulfate by human intestinal Caco-2 cells. Drug Metab Disp 34:1423–1431

Tamai I, Nezu J, Uchino H, Sai Y, Oku A, Shimane M, Tsuji A (2000) Molecular identification and characterization of novel members of the human organic anion transporter (OATP) family. Biochem Biophys Res Commun 273:251–260

Tamai I (2012) Oral drug delivery utilizing intestinal OATP transporters. Adv Drug Deliv Rev 64:508–514